Stratospheric variability and tropospheric ozone

Juno Hsu[1] and Michael J. Prather[1]

Received 5 August 2008; revised 11 December 2008; accepted 30 December 2008; published 17 March 2009.

[1] Changes in the stratosphere-troposphere exchange (STE) of ozone over the last few decades have altered the tropospheric ozone abundance and are likely to continue doing so in the coming century as climate changes. Combining an updated linearized stratospheric ozone chemistry (Linoz v2) with parameterized polar stratospheric clouds (PSCs) chemistry, a 5-year (2001–2005) sequence of the European Centre for Medium-Range Weather Forecasts (ECMWF) meteorology data, and the University of California, Irvine (UCI) chemistry transport model (CTM), we examined variations in STE O_3 flux and how it perturbs tropospheric O_3. Our estimate for the current STE ozone flux is 290 Tg/a in the Northern Hemisphere (NH) and 225 Tg/a in the Southern Hemisphere (SH). The 2001–2005 interannual root-mean-square (RMS) variability is 25 Tg/a for the NH and 30 Tg/a for the SH. STE drives a seasonal peak-to-peak NH variability in tropospheric ozone of about 7–8 Dobson unit (DU). Of the interannual STE variance, 20% and 45% can be explained by the quasi-biennial oscillation (QBO) in the NH and SH, respectively. The CTM matches the observed QBO variations in total column ozone, and the STE O_3 flux shows negative anomalies over the midlatitudes during the easterly phases of the QBO. When the observed column ozone depletion from 1979 to 2004 is modeled with Linoz v2, we predicted STE reductions of at most 10% in the NH, corresponding to a mean decrease of 1 ppb in tropospheric O_3.

Citation: Hsu, J., and M. J. Prather (2009), Stratospheric variability and tropospheric ozone, *J. Geophys. Res.*, *114*, D06102, doi:10.1029/2008JD010942.

1. Introduction

[2] Scientific efforts to understand the trends and variations in ozone observed over the past few decades have demonstrated the role of both photochemical and meteorological factors in driving stratospheric ozone change [e.g., *Randel and Wu*, 2007; *Stolarski et al.*, 2006; *Salawitch et al.*, 2005]. It has been proposed that these stratospheric changes have altered the tropospheric ozone burden over the past few decades [*Fusco and Logan*, 2003] and will continue to affect it in the future [*Sudo et al.*, 2003]. This paper presents a series of highly constrained modeling experiments that capture the observed trends and variations in stratospheric ozone and diagnose the corresponding changes in the stratosphere-to-troposphere flux of ozone. We are thus able to better understand the seasonal, interannual, and decadal trends in tropospheric ozone and the oxidative capacity of the lower atmosphere as driven by the stratosphere.

[3] The coupling of stratospheric and tropospheric ozone with chemistry models or with chemistry-climate models is occurring across the community [*Eyring et al.*, 2005]. These full models include a nearly complete set of chemical species and reactions that affect ozone, but are costly to run, and are often difficult to diagnose as to the causative factors of variability. We approach the problem with a simplified chemical model that is focused on simulating the stratosphere-troposphere exchange (STE) of ozone: a linearized ozone chemistry (Linoz version 1 [*McLinden et al.*, 2000]) combined with unique transport diagnostics that quantify the STE ozone flux as a function of time and place [*Hsu et al.*, 2005]. The Linoz model is revised (section 2) to use updated climatologies for background stratospheric composition and current photochemical data [*International Union of Pure and Applied Chemistry* (*IUPAC*), 2004; *Sander et al.*, 2006]. Stratospheric ozone simulated with the new Linoz version 2 in the University of California, Irvine (UCI) chemistry transport model (CTM) driven by Oslo European Centre for Medium-Range Weather Forecasts (ECMWF) Integrated Forecast System (IFS) meteorology data is tested against observed ozone climatology (section 3). The seasonal and interannual relationship between stratospheric ozone, STE ozone flux, and tropospheric ozone is derived for a continuous sequence of meteorological fields from January 2000 to December 2005 (section 4). The extent of the halogen-driven ozone STE decrease since 1979 is derived (section 5), and we discuss the overall role of the stratosphere in driving tropospheric ozone change (section 6).

[4] We find that stratosphere alone produces a peak-to-peak seasonal variation in tropospheric column ozone of about 7–8 Dobson unit (DU) at northern midlatitudes that parallels the late summer maximum normally attributed to

[1]Earth System Science, University of California, Irvine, California, USA.

0148-0227/09/2008JD010942

tropospheric photochemistry. The quasi-biennial oscillation (QBO) signature in total column ozone roughly matches that observed, and the QBO signals in STE ozone flux have maximum amplitudes in midlatitudes that are opposite in phase to its midlatitude QBO signal in total column ozone. The observed, post-1979 ozone depletion for the Northern Hemisphere (NH) can be best simulated in the UCI CTM with a 4K higher threshold activation temperature than the typical 195K threshold for polar stratospheric cloud (PSC) formation. Enhanced background bromine levels are found to have negligible effect on ozone depletion but our PSC chemistry is parameterized for fixed bromine and so only our non-PSC chemistry responds to enhanced Br_y. The maximum simulated decrease in the STE flux for post-1979 ozone depletion is about 10% in the NH and 22% in the Southern Hemisphere (SH). Furthermore, the latitude-season pattern of STE decrease due to ozone depletion is distinctly different from the pattern of change in total column ozone.

2. A Linearized Stratospheric Ozone Chemistry: Linoz Version 2

[5] Linoz is linearized ozone chemistry for stratospheric modeling [*McLinden et al.*, 2000]. It calculates the net production of ozone (i.e., production minus loss) as a function of only three independent variables: local ozone concentration, temperature, and overhead column ozone). A zonal mean climatology for these three variables as well as the other key chemical variables such a total odd-nitrogen methane abundance is developed from satellite and other in situ observations. A relatively complete photochemical box model [*Prather*, 1992] is used to integrate the radicals to a steady state balance and then compute the net production of ozone. Small perturbations about the chemical climatology are used to calculate the coefficients of the first-order Taylor series expansion of the net production in terms of local ozone mixing ratio (f), temperature (T), and overhead column ozone (c).

$$\frac{df}{dt} = (P-L)^o + \left.\frac{\partial(P-L)}{\partial f}\right|_o (f-f^o) + \left.\frac{\partial(P-L)}{\partial T}\right|_o (T-T^o) + \left.\frac{\partial(P-L)}{\partial c}\right|_o (c-c^o). \quad (1)$$

The photochemical tendency for the climatology is denoted by $(P\text{-}L)^o$, and the climatology values for the independent variables are denoted by f^o, c^o, and T^o, respectively. Including these four climatology values and the three partial derivatives, Linoz is defined by seven tables. Each table is specified by 216 atmospheric profiles: 12 months by 18 latitudes (85°S to 85°N). For each profile, quantities are evaluated at every 2 km in pressure altitude from z* = 10 to 58 km (z* = 16 km $\log_{10}$ (1000/p)). These tables are automatically remapped onto any CTM grid with the mean vertical properties for each CTM level calculated as the mass-weighted average of the interpolated Linoz profiles. Equation (1) is implemented for the chemical tendency in the CTM.

[6] We adopt the ozone climatology compiled by *McPeters et al.* [2007] which has improved profiles over the tropics and the SH from recent balloonsonde measurements from the Southern Hemisphere Additional Ozonesondes program. The temperature climatology is unchanged [*Nagatani and Rosenfield*, 1993]. The remaining chemical composition is specified as a climatology scaled to the tropospheric abundance of the long-lived source gases (i.e., N_2O, CH_4, and the halocarbons) so that it can be changed to reflect a changing atmosphere. This includes climatologies for three chemical families (NO_y = NO + NO_2+ HNO_3 + . . .; Cl_y = ClO + HOCl + $ClONO_2$+ HCl + . . .; Br_y = Br + BrO + $BrONO_2$ + . . .). We use N_2O as the primary measure of stratospheric composition and tracer-tracer relations to define the other trace gases. A monthly, latitude-by-height N_2O climatology above 22 km is based on CLAES satellite measurements (October 1991–May 1993 [*Randel et al.*, 1994]) and below 22 km is constructed from the compact correlation with O_3 from the NASA ER-2 in situ measurements in the lower stratosphere [*Strahan*, 1999]. The CH_4 and NO_y distributions are obtained using the polynomial fit with respect to N_2O from ATMOS measurements [*Michelsen et al.*, 1998a, 1998b]. The Cl_y climatology assumes conservation of halogens, thus increasing in the stratosphere as the organic source gases (e.g., CFCs, CH_3CCl_3, CCl_4) are photochemically destroyed [*Woodbridge et al.*, 1995]. The Br_y climatology likewise assumes increasing Br_y as the tropospheric bromine source gases (e.g., CH_3Br, CF_2BrCl, CF_3Br) are destroyed [*Wamsley et al.*, 1998]. For Br_y, we consider a sensitivity case where the tropopause value is increased to 6 ppt to include the relatively large amounts of inorganic bromine (Br_y) that may cross the tropopause [*Salawitch et al.*, 2005]. Water vapor adopts a lower boundary fixed at 3.65 ppm and follows conservation of potential water (H_2O +2xCH_4 = constant) throughout the stratosphere [*Nassar et al.*, 2005]. The tracer-tracer correlations are applied with N_2O scaled to the year of their observed correlations. Normalized distribution patterns for N_2O, CH_4, H_2O, NO_y and Br_y in January are shown in Figure 1. Tracer-tracer correlations derived from the more modern and complete observations yield trace gas distributions that are much improved compared with the ones used in the older version of Linoz.

[7] Ozone and temperature climatologies, to first order, determine stratospheric photolysis rates. We adopt a surface reflectivity of 0.3 as an average cloud cover. The photochemical box model is initialized with an approximate balance of species within each of the chemical families and integrated for 30 days to reach an approximate, diurnally repeating steady state, whereby the initialization of species within the families is, for the most part, forgotten. During this integration, the abundance of ozone and long-lived gases are fixed, and the chemical families are conserved. The net ozone production and three partial derivatives are evaluated numerically by perturbing the local ozone by +5%, the overhead column ozone by +5%, and the temperature by +4 K. The second-order terms in the Taylor expansion (equation (1)) are negligible for reasonable perturbations about the climatology [*McLinden et al.*, 2000, Figure 3].

[8] For Linoz version 2, the photochemistry has been updated from the 1997 vintage version 1 to current rate coefficients [*Sander et al.*, 2006] and cross sections [*IUPAC*, 2004]. New solar fluxes are taken from the average solar

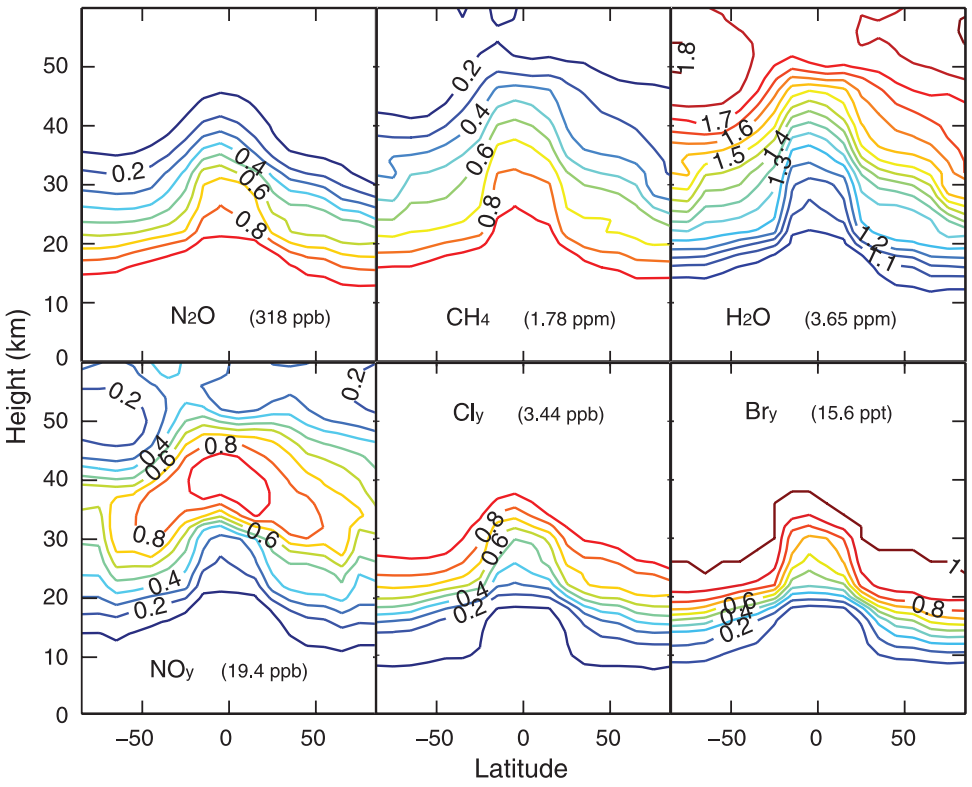

Figure 1. The Linoz climatologies of trace gases for January. For N_2O and CH_4, the patterns are normalized relative to their mean tropospheric abundances; for H_2O, the patterns are normalized relative to the tropopause value. The trace gas families (NO_y, Cl_y, and Br_y) are normalized relative to their maximum values (in the upper stratosphere). For year 2004, the normalization values are noted.

irradiance reference spectra derived by the SUSIM team for two different levels of solar activity [*Thuillier et al.*, 2004]. Compared to Linoz v1, these are 15–20% larger at wavelengths 177–200 nm, 5–10% larger at 200–300 nm, but relatively unchanged at wavelengths longer than 300 nm. Other notable updates affecting photolysis rates include the quantum yield of $O(^1D)$ from O_3 photolysis and the NO_2 cross sections.

[9] As an example of how the stratospheric chemistry model has evolved since v1, we follow the chemistry updates using a standard ATMOS profile (31 May, 30°N) from previous models and measurements studies [*Prather and Remsberg*, 1993]. The height profiles of net ozone production (P-L) and its derivatives with respect to ozone, temperature, and overhead column ozone are shown in Figure 2. A sequence of six model calculations are shown with successive updates tracking the change in chemistry from Linoz v1 to v2. Values generated with the JPL-1997 kinetics rates and cross sections and with the old solar flux data used for generating Linoz v1 are shown for comparison (JPL97-S3). Updating the quantum yields and cross sections only (JPL97-S2) has no effect on the three derivatives and a barely noticeable effect on net production, i.e., a small increase near 40 km. Updating the solar fluxes in addition (JPL97-S1) also has no effect on the derivatives but causes a large increase in net production throughout the stratosphere above 25 km. The update to JPL 2000 kinetics (JPL00-S1) causes a notable decrease in the temperature derivative between 34 and 48 km with an increase in net production from 34 to 44 km and a decrease below 34 km. Updating the kinetics to JPL 2002 (JPL02-S1) and JPL 2006 (JPL06-S1) has minor effects, with the latter causing a small decrease in net production about 30 km.

[10] The largest and most extensive changes in the chemical model occur in the net ozone production and not in the derivatives. The largest change in updating from JPL 1997 to JPL 2000 is caused by the addition of a new branch for the reaction, $OH + ClO \rightarrow HCl + O_2$. This new pathway weakens the Cl_y-catalyzed ozone loss and thus results in an increase in net production peaking around 38 km. The other major change with JPL 2000 kinetics was a stronger NO_y-catalyzed ozone loss from the increased kinetic rate for the reaction, $NO_2 + O \rightarrow NO + O_2$, and decreased kinetic rate for the reaction, $NO_2 + OH \rightarrow HNO_3$. Changes to chemical reaction rates after JPL 2000 have relatively minor effects on the ozone chemistry (outside of PSC conditions).

[11] Linoz v1 considered only non-PSC chemistry and did not include chlorine activation by polar stratospheric clouds (PSCs). Thus in v1, there was no Antarctic ozone hole and no enhanced Arctic loss during cold winters. In v2, we incorporate the PSC parameterization scheme of *Cariolle et al.* [1990] when the temperature falls below 195 K and the sun is above the horizon at stratospheric altitudes. The O_3 loss scales as the squared stratospheric chlorine loading (normalized by the 1980 level threshold). In this formulation PSC activation invokes a rapid e-fold of O_3 based on a photochemical model, but only when the temperature stays below the PSC threshold. It does not

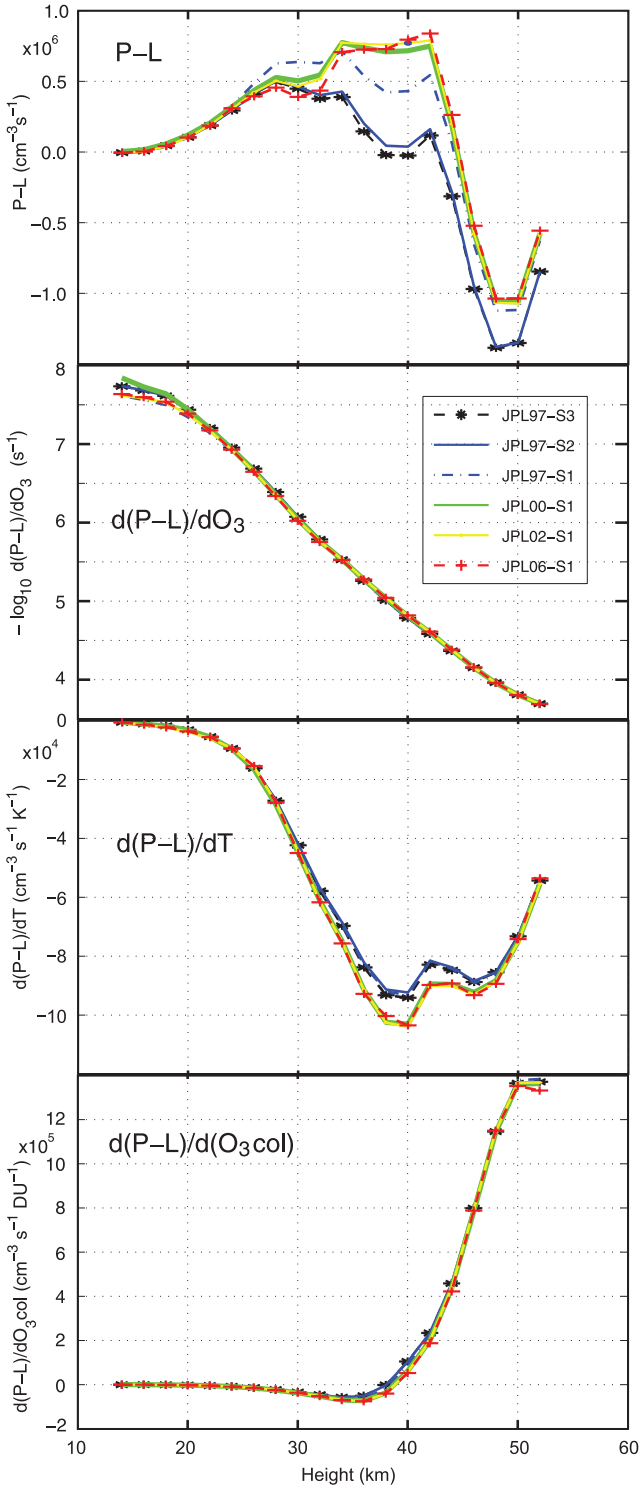

Figure 2. The sensitivity of Linoz terms (equation (1)) to different radiation and chemical updates using the standard ATMOS profile on 31 May at 30°N as the basic state. See text for details.

consider that the activated chlorine continues to destroy ozone for several days after encountering a PSC [*Schoeberl et al.*, 1993]. Recently, *Cariolle and Teyssedre* [2007] added a cold tracer to account for this effect. Their new parameterization, which is not used here, will be more important in the Arctic where PSCs are not sustained throughout the winter. In view of this process and the evidence of Cl_y activation on ternary aerosols at warmer temperatures [*Thornton et al.*, 2005], we test another version using a higher PSC activation temperature of 199K.

[12] Linoz chemical tendencies are applied only in the stratosphere, defined here as CTM grid points for which the O_3 abundance is greater than 100 ppb (10^{-7} moles per mole of dry air). These simulations do not include realistic tropospheric ozone chemistry, but instead invoke a parameterized sink that restores O_3 to 20 ppb in the lowest 600 m of the troposphere with an e-folding timescale of 2 days [*Hsu et al.*, 2005]. The choice of 20 ppb was made to imitate a more realistic chemistry and produce reasonable tropospheric column O_3. This tropospheric pseudochemistry is uniform, and thus variations in tropospheric O_3 calculated here are driven entirely by the STE ozone flux. When combining Linoz with a full tropospheric chemistry model, we simulate a separate Linoz tracer (O_3s) and use it every time step in each grid box to determine if the tropospheric chemistry is invoked (e.g., O_3s < 100 ppb) or if the Linoz net chemical tendencies are used (O_3s > 100 ppb).

[13] Using the normalized, monthly 2-D climatologies for stratospheric composition, we calculate five sets of Linoz v2 tables (see Table 1). Linoz-1979 uses the 1979 mean abundances from REF 1 of *Eyring et al.* [2005] and represents a stratosphere prior to significant ozone depletion. With Cl_y levels below the chlorine-loading threshold, PSC-induced loss is never invoked with Linoz-1979. Linoz-2004 uses year-2004 mean tropospheric abundances [*World Meteorological Organization*, 2007, Tables 1 and 2] and generates an Antarctic ozone hole. A second pair of Linoz tables, −1979Br and −2004Br, assume a 6ppt greater background of Br_y throughout the stratosphere [see *Salawitch et al.*, 2005]. We also use the Linoz-2004Br tables with a warmer PSC threshold of 199K and denote this case as Linoz-2004BrT. Note that the Linoz tables assume only gas phase chemistry plus some sulfate reactions (N_2O_5+aerosol, $BrONO_2$+aerosol) using year 1990 of the SAGE II climatology [*Thomason et al.*, 1997] for the aerosol surface area. Without very cold, ternary-aerosol chemistry, ClO levels in the lower stratosphere are always low and the additional background Br_y does not notably enhance ozone loss.

3. Evaluating Column Ozone With Linoz

[14] To assess the impact of the updated Linoz v2 on stratospheric ozone, we repeat the Linoz v1 simulations of *Hsu et al.* [2005] with Linoz-2004 and the Oslo/EC meteorology for year 1997 derived from the ECMWF IFS Cycle 23r4. Linoz v1 is known to be biased low in column O_3 in the tropics and high in high latitudes [*Wild et al.*, 2003, Figure 1]. With Linoz-2004 this bias is mostly eliminated: tropical ozone columns increase by 5–20% for all but the northern winter, and outside of the tropics ozone is reduced by similar percentages for all months except December. In terms of STE, if we run Linoz-2004 tables but turn off the PSC parameterization, the O_3 flux increases by 9% from 516 Tg/a (Linoz v1 tables) to 563 Tg/a, with greater increases in the SH. The spatial and temporal STE patterns remain roughly the same. Inclusion of the parameterized

Table 1. Prescribed Abundances of Long-Lived Species and Activation Temperatures for the PSC Parameterization Used for Deriving the 5 Linoz Tables Indicated in the Column Heading[a]

Species Abundances Linoz v2	Linoz-1979	Linoz-2004	Linoz-1979Br	Linoz-2004Br	Linoz-2004BrT
N_2O (ppbv)	300.4	318.4	300.4	318.4	318.4
NO_y (ppbv)	18.2	19.4	18.2	19.4	19.4
Cl_y (pptv)	2242	3437	2242.	3437	3437
Br_y (pptv)	8.7	15.6	14.7	21.6	21.6
CH_4 (ppbv)	1555	1777	1555	1777	1777
H_2O (ppmv)	3.65	3.65	3.65	3.65	3.65
PSC activation temperature (K)	NA	195	NA	195	199

[a]Note that the PSC parameterization is not used for pre-ozone depletion runs (Linoz-1979 and Linoz-1979Br). See text for details.

PSC chemistry with Linoz-2004 reduces the STE ozone fluxes globally by 10%, again with greater response in the SH. The total shift in STE ozone flux from v1 to v2 (Linoz-2004) is +3% in the NH and −7% in the SH. Thus the changes in the photochemical data and inclusion of a parameterized PSC loss have corrected the prominent biases in Linoz v1 but the total STE ozone flux is only slightly reduced.

[15] Stratospheric column O_3 calculated with Linoz-2004 with 1997 ECMWF IFS Cycle23r4 meteorological data are compared with those from observations [*McPeters et al.*, 1997, 2007] in Figure 3. We show results for both with and without PSC parameterization. For both CTM and observations, the stratosphere is defined as where O_3 abundances exceed 100 ppb. The observed climatology compiled by *McPeters et al.* [2007] is an improvement over the climatology compiled by *McPeters et al.* [1997], but the changes also reflect the inclusion of more recent years with greater ozone depletion, e.g., a deeper Antarctic ozone hole in September and greater Arctic loss in March. From 40°S to 40°N, the Linoz simulation is excellent, with no obvious biases and errors less than 25 DU. At high latitudes, the PSC parameterization in general improves the Linoz simulations, particularly for the SH ozone hole. However, the model-climatology comparison in Figure 3 looks bad in polar regions for some months, due in part to the circulation (e.g., the model's seasonal recovery from the Antarctic ozone hole is too rapid) and in part to the observations being extrapolated (e.g., 70–90 N in December). The comparison is also for only one year of EC meteorology and a better comparison of the seasonality in total column O3 is presented in Figure 4 below.

[16] To study interannual variability we use continuous ECMWF IFS T42L40 meteorological fields from years 2000 through 2005. Year 2000 data are extracted from ECMWF IFS Cycle 23r4 model whereas the rest are extracted from Cycle 29r2 model. We find Cycle 29r2 generates about 20% more STE flux than does version Cycle 23r4 (see below), and this difference is much greater than the interannual variability. Thus year 2000 meteorological data are only used to spin up the experiments to approach a steady state before continuing with the next five years from January 2001 through December 2005, which are analyzed here. This five-year monthly mean climatology of total column O_3, plus the interannual variability defined relative to the five-year mean, are compared with the recent corrected Earth Probe TOMS observations based on NOAA-16 SBUV/2 ozone records as shown in Figure 4. Note that the missing data for December 2005 are replaced with those from December 2004 for convenience. This CTM simulation with Linoz-2004 captures the general patterns of the observed seasonal cycle and the Antarctic ozone hole with its minimum below 190 DU. At mid and high northern latitudes, total column O_3 is well simulated. In the tropics, the minimum (NDJF at 15°N) are likewise matched, but the CTM has a spurious high (310 DU contour) in July at 10°N and likewise with 270 DU contour bulging equatorward to 10°S in austral summer. Even worse, the circum-Antarctic maximum around 60°S is consistently about 60 DU higher than observed. These anomalies do not appear in the previous publications with Linoz v1 using the 1997 and 2000–2001 Cycle 23r4 meteorological data. Using Linoz-2004BrT reduces the total ozone error by 20 DU confined to poleward of 60°S and over the spring Arctic vortex. The spurious errors remain evident and large regardless of the chemistry used.

[17] Analysis of the monthly latitude-height ozone profiles from the CTM (not shown) reveals a deep sinking motion near the edge of the Antarctic polar vortex that persists through the seasons and a spurious downward shift of contours in the top model layers at 10°N in July and 10°S in January. We presume these errors stem from a poorly resolved stratosphere with a top lid in the middle stratosphere (2 hPa). To test this point, we acquired year 2005 using IFS Cycle 29r2 but with much finer vertical resolution, T42L60, in which the whole stratosphere is resolved with layers at most 1.5 km thick from 15 to 0.5 hPa. Linoz-2004 with the T42L60 meteorological data corrects the worst errors seen with the T42L40 meteorological data as shown in Figure 5, namely, the tropical bubble disappears and the circum-Antarctic high columns now are lower and closer to observations. Unfortunately, the T42L60 data was only available to us for year 2005, and so our analysis of interannual variability continues with the T42L40 data.

[18] Monthly anomalies in zonal mean total column O_3 for years 2001–2005 are shown in Figures 4c and 4d. In October 2002, the CTM matches the extremely high column anomaly over Antarctica, which was caused by a sudden warming event and the transport of ozone-rich air into the vortex [e.g., *Simmons et al.*, 2005]. In general the phases of alternating high and low anomalies are well captured by the CTM and a two-year QBO-like signal is evident. In spite of the coarsely resolved lower stratosphere, the ECMWF IFS 40-layer model produces a QBO with alternating descending easterlies and westerlies in the stratosphere (not shown). The forecast model is reinitialized with observations every 24 hours and appears to generate a QBO pattern in the lower stratospheric transport. The magnitude of the modeled

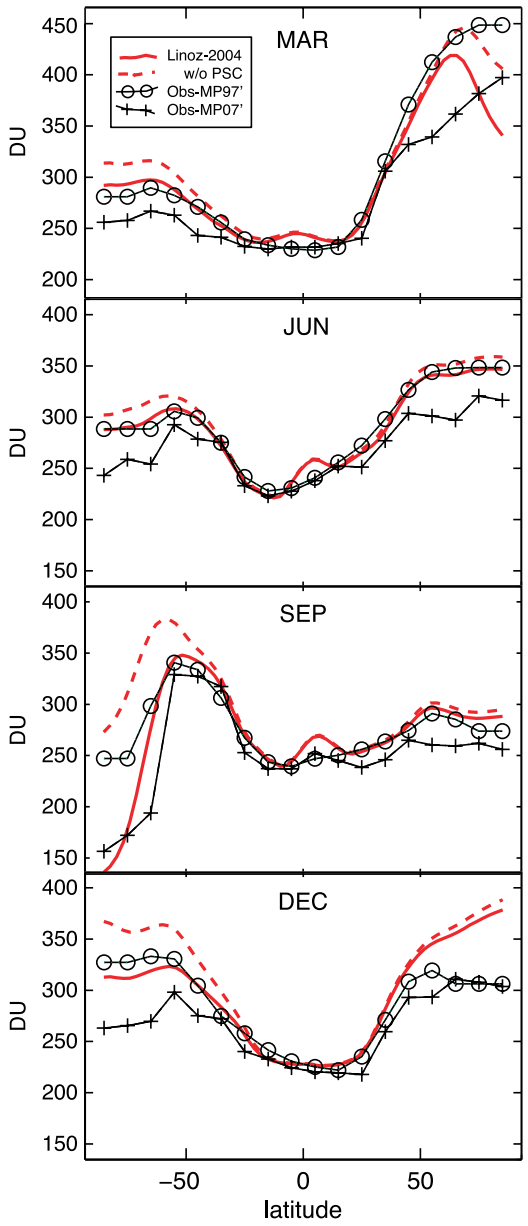

Figure 3. Stratospheric column O_3 (DU) as a function of latitude for March, June, September, and December. The stratospheric column is integrated over the atmosphere where O_3 > 100 ppb. The four different profiles are climatology compiled by *McPeters et al.* [1997] (black line with o(tm)), climatology compiled by *McPeters et al.* [2007] (black line with +(tm)), simulation with Linoz-2004 in the UCI CTM with the 1997 ECMWF IFS meteorology data (red solid line), and the same Linoz-2004 simulation but without PSC parameterization (red dashed). See text for details.

equatorial and SH interannual variability in O_3 column, however, is often twice as large as observed.

[19] To understand the modeled interannual variability and its relation to the STE O_3 flux, we isolate the QBO signal following the regression procedure of *Randel and Wu* [1996]. A QBO time series is defined by determining the linear combination of the equatorial zonal wind at 20 and 40 hPa that best correlates the equatorial total column O_3 interannual variability. This time series is then regressed against the time series of total column O_3 anomalies at all latitudes (Figure 4d). Figure 6 shows (1) the modeled total column O_3 anomalies associated with the QBO and (2) the residuals. The QBO signal in total column O_3 shows large positive (negative) equatorial ozone anomalies during equatorial westerlies (easterlies) as observed. The subtropical QBO signal is correctly out of phase with the equatorial signal. However, this signal is more confined to the subtropics than is observed [*Randel and Wu*, 1996, Figure 1], and the observed 6-month phase lag between the maxima at subtropical and mid latitudes in the two hemispheres is absent. Also unlike earlier observations [e.g., *Randel and Cobb*, 1994], the SH midlatitude QBO signal does not continue into to the spring Antarctic polar region but directly changes sign before 60°S. This points to the possibility that for the coarsely resolved stratosphere of the ECMWF L40 model, the interaction of the annual cycles and the QBO as well as the high-latitude planetary waves modulated by the QBO [see *Baldwin et al.*, 2001] are completely missing or even misrepresented. The residuals are about the same magnitude as the QBO signal and show a large-scale, low-frequency, coherent structure in the SH that is roughly out of phase with the structure at the equator.

4. STE Ozone Flux and Tropospheric Ozone

[20] Following *Hsu et al.* [2005], the STE ozone flux is calculated based on the mass balance of each latitude-by-longitude tropospheric ozone column on the CTM grid points. The net STE ozone flux is the residual from three terms computed hourly: the change in tropospheric ozone mass, the flux divergence of tropospheric ozone (i.e., air mass with abundance <100 ppb) and the parameterized ozone sink in the lowermost layers. In this study, the diagnostic is further improved by using the first moment of the horizontal ozone flux to determine the fraction of the ozone flux being advected to a neighboring CTM box that is tropospheric (i.e., <100 ppb) whereas in the previous study only the mean abundance of the advective flux is used. This improvement has greatly reduced the overall noise level such as the dipole structures within the Pacific jet stream noted in the previous study. Figure 7 shows the averaged seasonal cycle of STE O_3 fluxes calculated from the CTM simulations with Linoz-2004 from years 2001–2005 (white contour lines) along with the average zonal mean zonal wind at 200 hPa (shaded contours). Similar to the year 1997 and 2000/2001 results [*Hsu et al.*, 2005, Figure 10], the STE maximum in the NH occurs just poleward of the tropospheric zonal jet, peaks during late spring and early summer when the zonal jet weakens, and migrates with the subtropical jet up to 45°N. In the SH, the STE maximum stays around 30°S, does not migrate poleward with the jet in summer, but does peak during austral spring when the jet weakens. However, the global STE flux is on average 20% larger than the previous estimates [*Hsu et al.*, 2005] despite the fact that as discussed in section 3, the global STE flux should be slightly reduced using Linoz-2004 and including the PSC parameterization. The larger magnitude is mostly due to the excessive descent in the Antarctic circumpolar region with the Cyc29r2 L40 fields as already seen in total

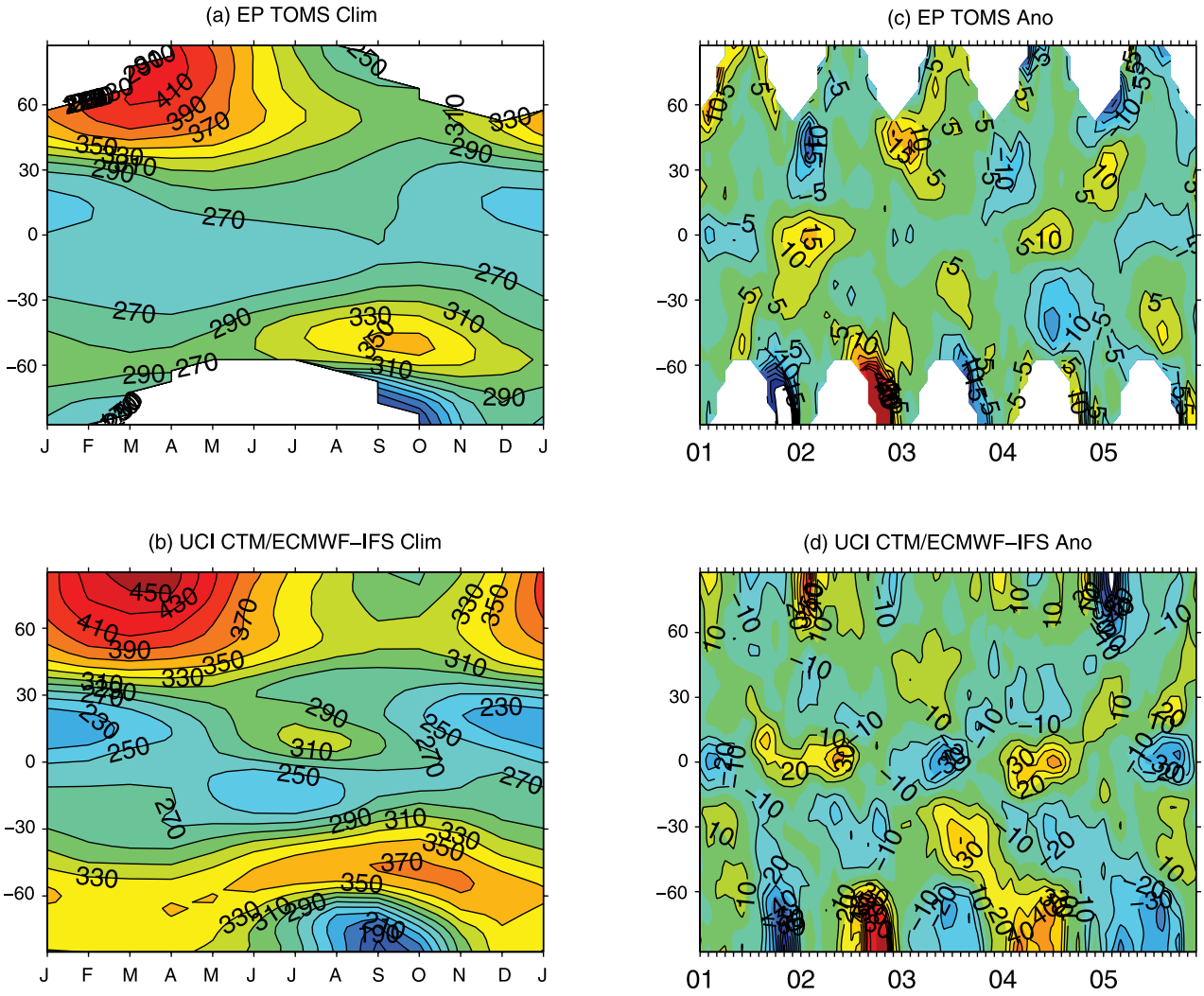

Figure 4. Five-year (2001–2005) monthly zonal mean climatology of total column O_3 (DU) as a function of latitude and for (a) corrected Earth Probe TOMS and (b) Linoz-2004 CTM simulation using Oslo/EC meteorological data at T42L40 resolution from IFS Cycle 29r2. The anomalies relative to these climatologies from January 2001 to December 2005 are shown for (c) TOMS and (d) CTM. Contour intervals for the CTM simulation anomalies are 10 DU, but those for the TOMS anomalies are only 5 DU.

column ozone discussed above. Indeed, recalculating the STE flux using the ECMWF 2005 Cyc29r2 L60 data, we find that the L40 SH STE flux is about 25% too large.

[21] The QBO's role in modulating the STE O_3 flux is derived with the same method as for total column O_3. STE variability attributed to the QBO (Figure 6c) is small: peak contour intervals in midlatitudes are +0.20 g m^{-2} a^{-1} (30°S in 2004) as compared with a global average of about 1.2 g m^{-2} a^{-1} (i.e., 610 Tg per year). These midlatitude STE QBO signals are out of phase with the midlatitude total column ozone QBO, and, not surprisingly, there are no QBO signals over the tropics and high latitudes where STE ozone fluxes are negligible. This pattern indicates that the induced sinking part of the overturning circulation in the subtropics during the easterly phase of QBO creates a dynamical condition that disfavors the mixing of the mid-latitude, lower stratospheric ozone into the troposphere. The STE residual field (Figure 6d) has much larger amplitudes than the QBO signal. In SH both STE and total column O_3 residuals show the same low-frequency variability. At 35°S, they are positively correlated with a maximum correlation coefficient 0.44 with STE lagging total column ozone residual by 9 months. This relationship is mostly evident between the positive total column ozone anomaly in June 2003 (red patch, Figure 6b) followed by the positive STE anomaly (red patch, Figure 6d) in early 2004. However, a longer data set will be needed to confirm its significance. In the NH, the STE residuals lack coherence and have smaller amplitudes.

[22] Influx of O_3 from the stratosphere is a principal component of the tropospheric O_3 budget, the others being in situ photochemical production and loss and surface deposition. The amount of tropospheric O_3 that can be assigned a stratospheric origin, however, is not well defined. There is a wide range of reported STE fluxes and various accounting methods for tropospheric production and loss

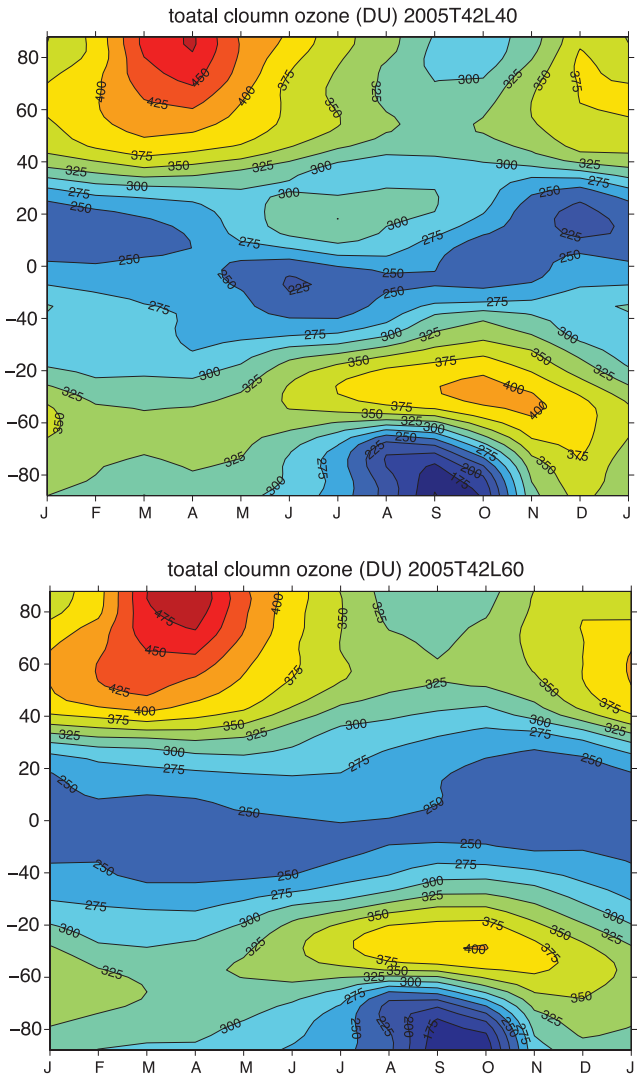

Figure 5. Year 2005 monthly zonal mean total column O_3 (DU) simulated with Linoz-2004 for (top) T42L40 CTM and (bottom) T42L60 CTM.

[e.g., *Prather et al.*, 2001; *Stevenson et al.*, 2006]. In this study, we quantify the variability in tropospheric O_3 caused by changes in STE by using a simplified, uniform chemistry in the troposphere, namely, O_3 in the lowest 600m is relaxed toward 20 ppb. We diagnose tropospheric column O_3 (adopting common usage of TCO for the tropospheric column ozone) hourly as the vertically integrated ozone burden for all CTM layers with abundances less than 100 ppb. Thus, with these simulations, the latitudinal and seasonal variations in TCO (color-filled contours in Figure 8a) are driven by STE ozone flux (line contours in Figure 8a). In the NH, the monthly zonal mean TCO varies from 16 to 26 DU with lowest values in the tropics (where the troposphere is largest). In northern midlatitudes, the seasonal peak-to-peak range is 8 DU, and although this tends to follow the troposphere mass (i.e., the tropopause peaks in late summer) a large fraction appears to follow the STE ozone flux. This large seasonality is driven without tropospheric chemistry. We expect the TCO to lag the STE by a month (i.e., the tropospheric lifetime of an STE perturbation, see section 6 for more discussion).

[23] Comparing to the recently observed TCO derived from OMI and MLS measurements [*Ziemke et al.*, 2006, Figure 6], our modeled TCO without tropospheric chemistry surprisingly matches the observed latitude-by-month pattern, much better than the comparison with the full chemistry CTM by Ziemke et al. Our TCO is, however, consistently biased low by about 8 DU over the tropics and wintertime midlatitudes. Furthermore, we underestimate the magnitude of the buildup to maximum TCO seen at 40°N in July and at 30°S in November by 18 DU, indicating the importance of tropospheric photochemical net production that is not simulated here. Renormalizing the TCO pattern to the tropospheric mass shows the variation in mean tropospheric ozone abundance (ppb in Figure 8b). Here, we see that peak abundances tend to follow the STE ozone flux. Given that the tropospheric parameterization pushes to a uniform mixing ratio, this simulation provides a measure of the seasonality and amplitude of tropospheric O_3 variability driven by STE.

5. Ozone Depletion and STE Ozone Fluxes

[24] The reduction in STE O_3 flux from the halogen-catalyzed depletion of stratospheric O_3 is evaluated with different Linoz v2 models. We simulate predepletion O_3 with Linoz-1979 using the meteorological data for years 2001–2005. For postdepletion, we use the same meteorological data and Linoz-2004. Additional experiments, Linoz-2004Br and Linoz-2004BrT are used to investigate the effect of enhanced bromine background and higher PSC temperature threshold for post-ozone depletion. Because the additional bromine represents a natural tropospheric source, we simulate the predepletion ozone, Linoz-1979Br to be paired with the latter experiments. Note that because we have only meteorological data for recent years, this study cannot elucidate the role of changing transport in the observed depletion.

[25] All three Linoz variants (2004versus1979, 2004Brversus1979Br and 2004BrTversus1979Br) calculate qualitatively similar latitudinal patterns of column O_3 depletion as observed in the merged satellite data based on TOMS/SBUV measurements from 1979–2000, e.g., maximum NH spring depletion of about 6% per decade in the polar region [*Fioletov et al.*, 2002, Figure 11]. All Linoz simulations show largest depletion in spring and in winter over the polar region of each hemisphere. However, the magnitude of the overall ozone depletion and the difference between the strong spring/winter depletion and the weak fall/summer depletion in the NH, are largely underestimated unless the activation temperature of the PSC parameterization is raised from 195K to 199K. Additional bromine background has only a small effect on further ozone depletion in these calculations compared to those of *Salawitch et al.* [2005]. As noted before, we speculate that this could be the result of our PSC parameterized loss being independent of bromine level.

[26] Figure 9 shows the latitude-by-month changes in total column O_3 (DU) and STE O_3 flux (g m^{-2} a^{-1}) between Linoz-1979Br and Linoz-2004BrT for the five year average of 2001–2005 meteorology. We can compare

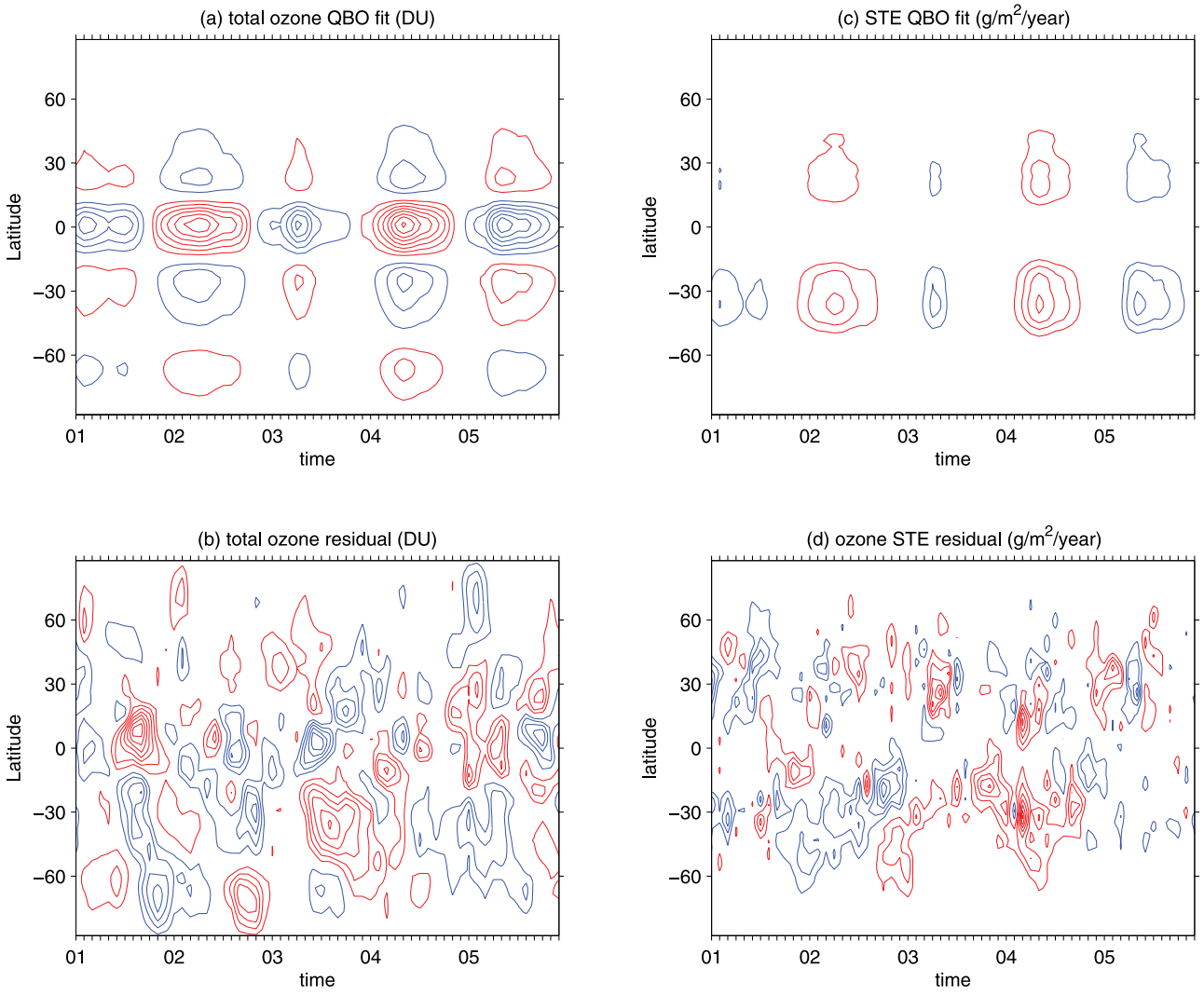

Figure 6. Monthly zonal mean anomalies in the modeled total column O_3 split into (a) QBO signal and (b) residuals, taken from the 2001–2005 simulation shown in Figure 4d. Contour intervals are +5, +10, and +15 DU (solid red) and −5, −10, and −15 (dashed blue). Corresponding monthly zonal mean anomalies in the STE O_3 fluxes are shown for (c) QBO signal with contour intervals of ±0.05 g m^{-2} a^{-1} and (d) the residuals with contour intervals of ±0.10 g m^{-2} a^{-1}. Zero contour lines are omitted.

the ozone depletion in Figure 9a directly to the vertically integrated SAGE/sonde stratospheric ozone data over 1979–2005 [*Randel and Wu*, 2007, Figure 10]. Overall, the simulations agree with observations, both in shape and magnitude. In the tropics, the difference of about 8 DU in total column O_3 relative to the pre-ozone depletion is as large as seen in SAGE/sonde data [*Randel and Wu*, 2007, Figure 10a], but disagrees with the equatorial total ozone change of about zero seen in the merged TOMS/SBUV data [*Randel and Wu*, 2007, Figure 10b]. In our simulation at T42L40, the top layer from 2 to 20 hPa does not accurately cover the diversity in upper stratospheric O_3 chemistry whereby chlorine-driven depletion above 3 hPa results in more penetration of solar ultraviolet and hence more O_3 production below. Other errors in our simulation include: missing the second maximum in NH ozone depletion during the fall; and simulating Antarctic ozone depletion to be about twice as large as the observed. The latter discrepancy could be reduced if there were some PSC-induced ozone loss already in 1979, which is not modeled here.

[27] The latitude-month change in the STE ozone flux is quite different from that in total column ozone. For the NH STE change, the difference pattern follows roughly the seasonal pattern in Figure 7 but with the maximum depletion in summer lagging the seasonal STE maximum by 2 months. The maximum change in the NH STE ozone fluxes is about −0.3 g m^{-2} a^{-1} (less than 10% change) and is about twice that obtained when the PSC threshold is lowered to 195 K. The SH STE change pattern does not resemble its seasonal pattern. The maximum decrease, −0.7 g m^{-2} a^{-1}, occurs in the austral summer around 40°S with a six month time lag from the Antarctic ozone hole. Antarctic ozone, primarily in the isolated vortex, requires more time to propagate to the midlatitudes than its NH counterpart.

[28] Figure 10 shows the seasonal changes in the ozone vertical profiles at NH mid latitudes for all three pairs of

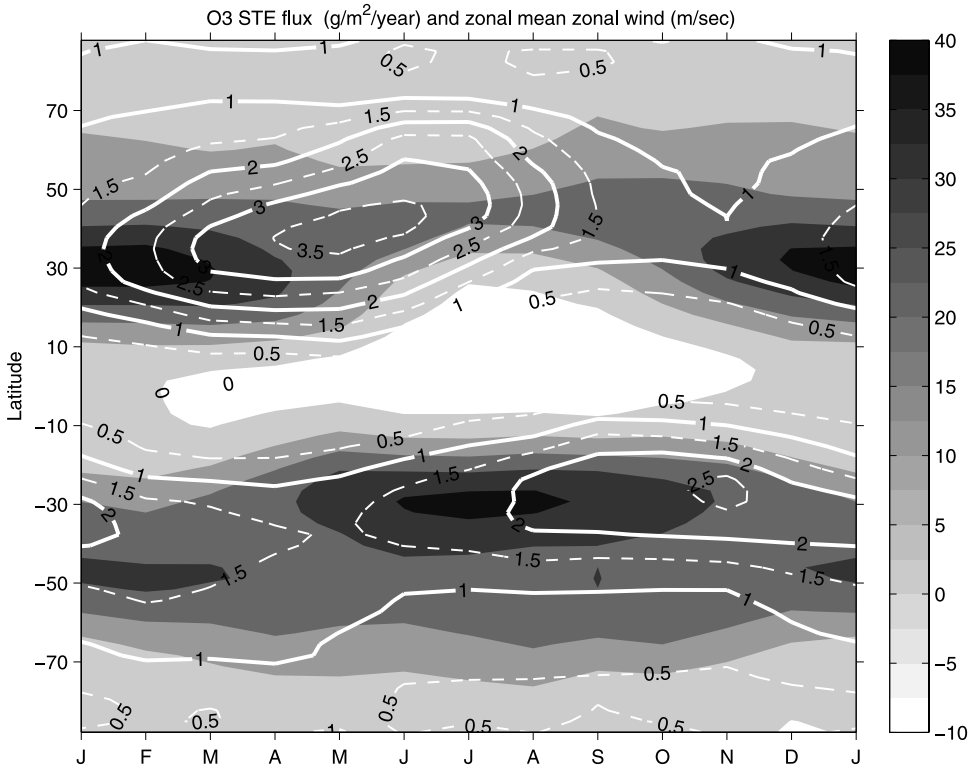

Figure 7. Latitude-by-month average STE O_3 fluxes (white line contours at 0 to +3.5 g m^{-2} a^{-1}) from UCI CTM with Linoz-2004 driven by ECMWF IFS T42L40 2001–2005 meteorological data. Zonal mean zonal wind at 200 hPa (gray scale contours at −5, +5, +15, +25, and +35 ms^{-1}) from the same meteorological data.

experiments. Decreases are most evident near 11–14 km in the lower stratosphere as the peak moves down in height from spring to summer. The annual maximum decrease in the lower stratosphere from Linoz-2004BrT minus its pre-ozone depletion run, Linoz-1979Br, is about 11%. This trend corresponds to about 8% per decade for the 1979–1990 period assuming that the total change in ozone between 1979 and 2004 is about 1.4 times the linear trend values for 1979–1990 (as stated in the study of *Randel and Wu* [2007]). It is comparable to the about 7.3% per decade estimates for a similar period [*Randel et al.*, 1999] but is much smaller than the 30% decrease, estimate from 1970s to mid 1990s reported by *Fusco and Logan* [2003]. With Linoz-2004Br minus Linoz-1979Br, the net ozone depletion is at most 5%. The relatively uniform and weak decrease in the NH winter seen in Figure 10 is distinctly different from the profiles of the other seasons and from observations. It might point to the importance of a trend in winter circulation [*Hood and Soukharev*, 2005] lacking in this study.

6. Discussion and Conclusions

[29] To separate changes in STE ozone flux due to ozone depletion from those due to natural variability, we construct a regression model for the hemispheric monthly STE flux from the five-year sequence for each of the Linoz runs. The STE data are fitted to a hemispheric mean, the seasonal harmonics and the three time series of the QBO, the Arctic Oscillation (AO [*Thompson and Wallace*, 1998]) and the El Niño Southern Oscillation (ENSO) index [*Ziemke and Chandra*, 2003]. The fitted mean and the amplitude of the seasonal cycle decrease in response to changes in halogen loading and the PSC chemistry among different Linoz runs. However, the interannual variances are rather insensitive to the chemical change, thus we use the average percentage change from all model runs for describing the interannual variances.

[30] The QBO accounts for about 20% of the NH interannual variances in STE. Including the AO decreases the unexplained interannual variances only by 2–3%. The total NH interannual variability is about 25 Tg/a (root-mean-square [RMS]), the same as the long-term change driven by ozone depletion (Linoz-2004BrT minus Linoz-1979Br). Thus, as detection of a NH trend in column ozone is obscured by transport variability [e.g., *Stolarski et al.*, 2006], so is any long-term change in STE flux. The SH STE flux shows quite different modes of variability. For the SH regression model, we replace the AO index with the AAO (Antarctic Oscillation [*Thompson and Wallace*, 1998]) index. The QBO nearly captures about 45% of the interannual variability, while the AAO captures negligible variance and thus does not contribute to coherent structure of the residuals seen in Figure 6d. The maximum SH STE trend due to ozone depletion (70 Tg/a) is twice as large as the interannual variability (30 Tg/a RMS) over the years 2001–2005. Including the ENSO index in either hemisphere does not decrease the unexplained interannual variances. In our model the deseasonalized ENSO index correlates poorly with either hemispheric STE or global STE anomalies in

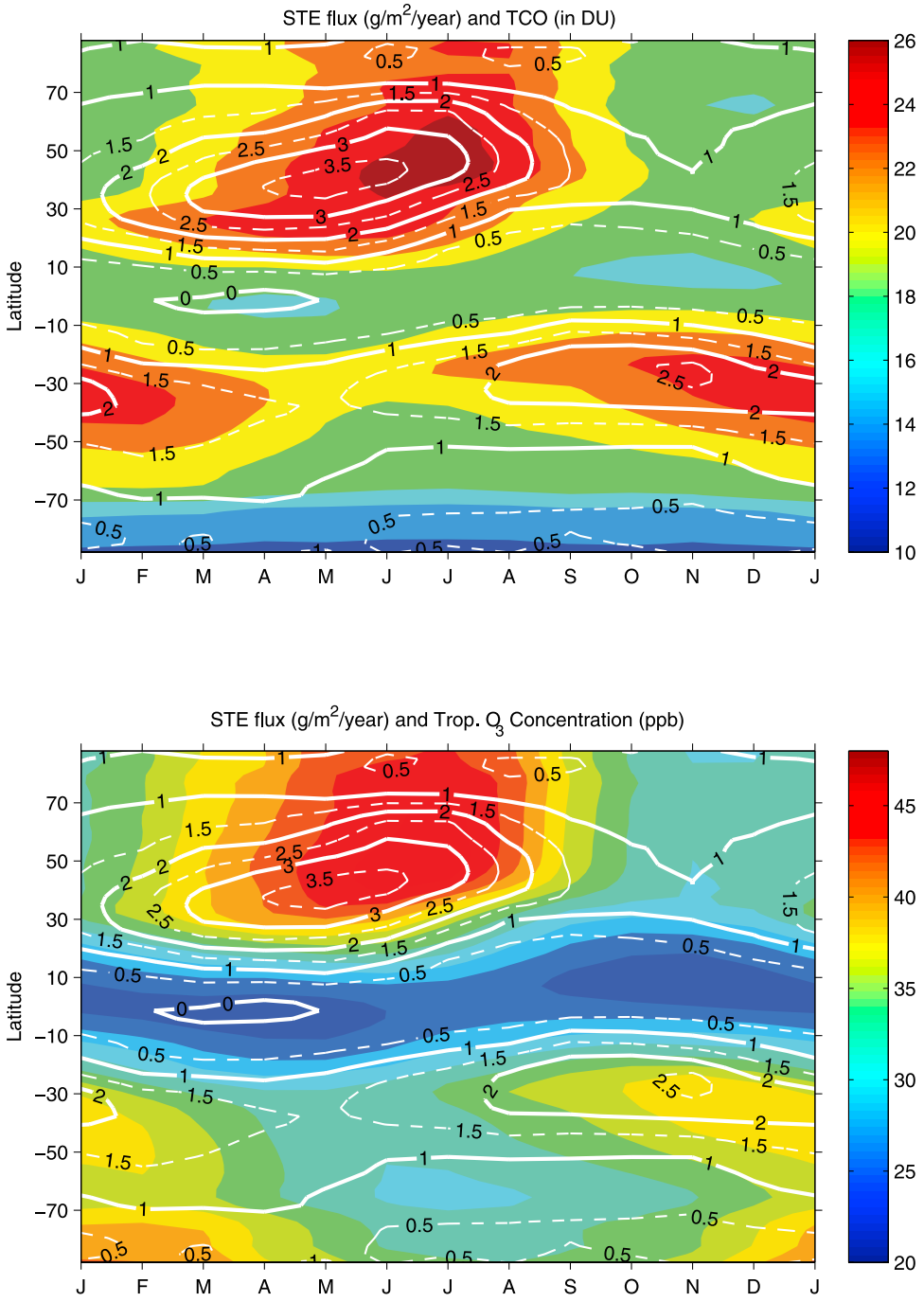

Figure 8. (top) Latitude-by-month average STE O_3 fluxes (see Figure 7) on top of simulated tropospheric column ozone (TCO, color-filled contour interval, 2 DU) for Linoz-2004 simulations. (bottom) Same STE O_3 fluxes on top of monthly zonal mean tropospheric O_3 abundance (in parts per billion) with color-filled contours interval, 2 ppb.

lagged correlations between ±6 months. The correlation remains poor even after we remove the influence of the QBO from the STE time series. The 2002–2003 El Niño is readily apparent in our ECMWF meteorological fields but does not enhance the STE O_3 flux in our model. In contrast, *Zeng and Pyle* [2005] found a high anticorrelation between ozone STE anomalies and the ENSO index six month earlier from 1990–2001.

[31] The impact of changes in the STE flux on tropospheric ozone is shown with the scatterplot of the seasonal hemispheric STE fluxes (Tg/a) versus the hemispheric tropospheric ozone burden (Tg) for all 25 years of Linoz v2 simulations for December-January-February (DJF) and June-July-August (JJA) (Figure 11). The linear correlations is obvious, particularly for the winter season of each hemisphere. The slope of the scatterplot reflects the lifetime

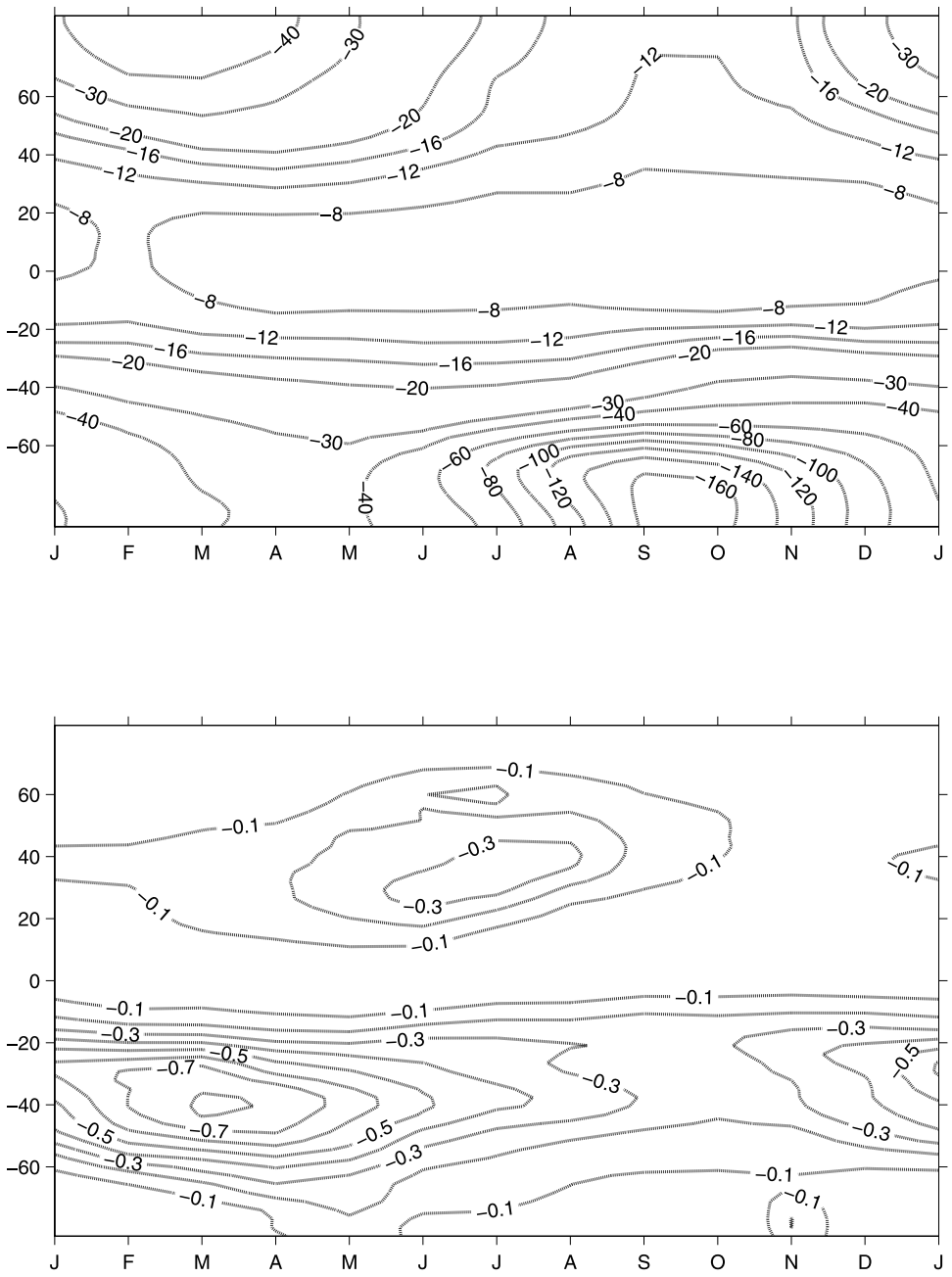

Figure 9. (top) Monthly zonal mean differences in total column O_3 (DU) for Linoz-2004BrT minus Linoz-1979Br. Both Linoz simulations are driven by the same 5-year ECMWF IFS data from 2001 to 2005. (bottom) Monthly zonal mean differences in STE O_3 flux (g m^{-2} a^{-1}) for Linoz-2004BrT minus Linoz-1979Br.

of the perturbations to tropospheric ozone. The NH seasonal lifetime of tropospheric ozone varies from 28–39 days, longest for fall and shortest for spring with an annual mean of 35 days. The lifetimes for the SH have less seasonal variation and are slightly shorter, varying from 27–32 days with an annual mean of 30 days. Our simplified troposphere chemistry allows air of stratospheric origin to wander freely in the troposphere until reaching below 600m altitudes where the O_3 abundance is reset rapidly to 20 ppb. Thus the lifetime of about one month reflects mostly the characteristics of the tropospheric circulation and mixing and is slightly longer than the estimate of 22 days for all of tropospheric ozone from the multimodel ensemble simulations with full tropospheric chemistry [*Stevenson et al.*, 2006]. Realistic loss of stratospheric ozone, occurring throughout the free troposphere, is not simulated in our model. These results, however, will provide a baseline for a corresponding study (in prep) in which the full tropospheric chemistry is included. The intercepts of the scatterplots at zero STE flux reflect our adopted 20-ppb ozone restoring term in the lowermost layers and are higher (in Tg) in summer because of the larger tropospheric volume (higher tropopause). Thus the

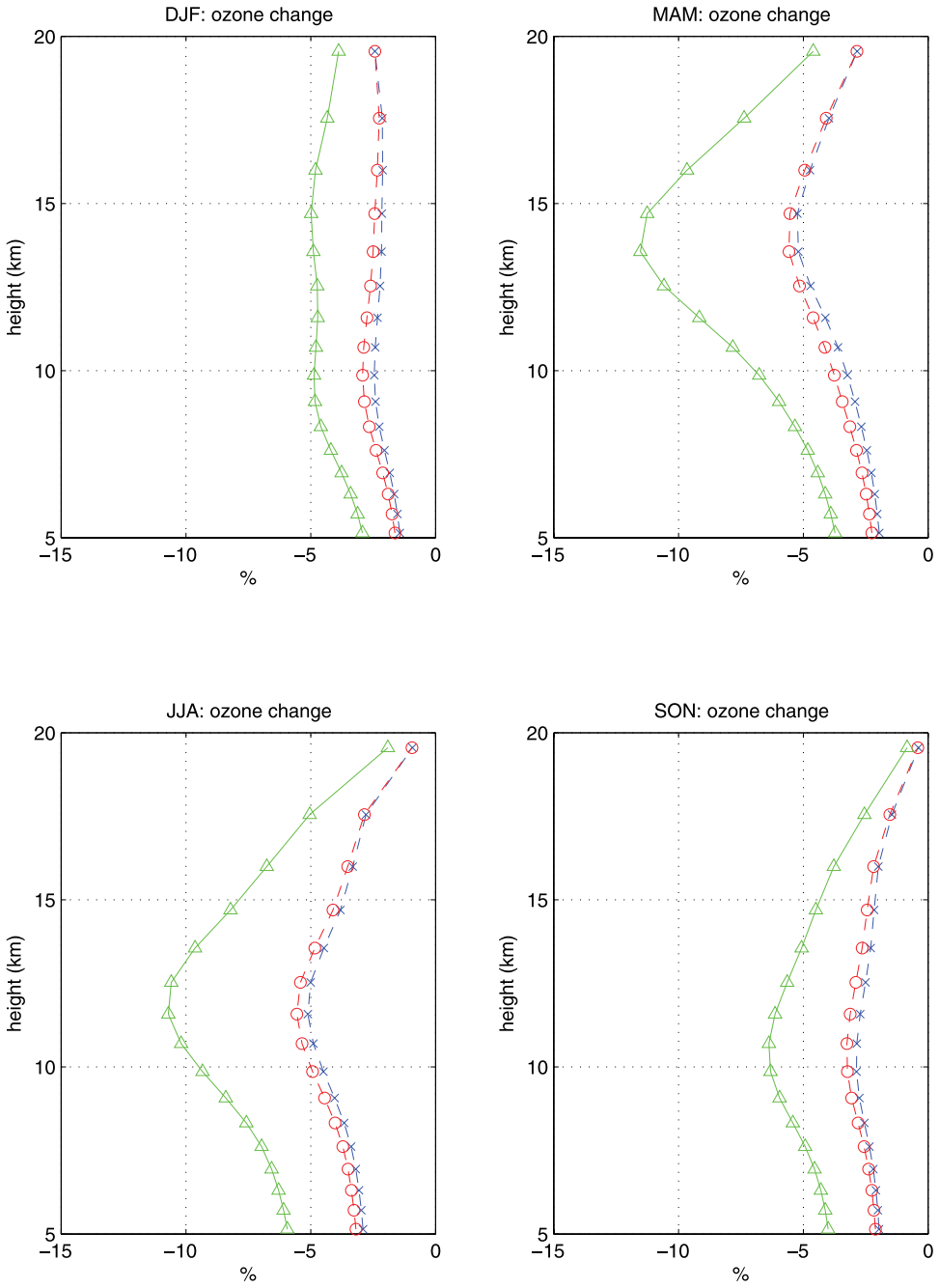

Figure 10. Seasonal profile changes in O_3 abundance (%) over the lower stratosphere and upper troposphere at 40°N–50°N for all Linoz-2004 runs minus their respective pre-ozone depletion runs. Linoz-2004 minus Linoz-1979 (crosses), Linoz-2004Br-Linoz-1979Br (circles), and Linoz-2004BrT minus Linoz1979Br (triangles). All calculations use the same meteorological data.

total ozone burden and absolute STE ozone flux cannot be used to derive a lifetime.

[32] The interannual variability is similar across all model runs regardless of the chemistry, as seen in the similar scatter pattern from each Linoz run. The interannual variability between NH and SH appears uncorrelated. The mean decrease in STE flux due to ozone depletion between Linoz-1979Br and Linoz-2004BrT in the NH is 25 Tg/a, corresponding to less than 1 ppb decrease in mean abundance and that in the SH is 72 Tg/a, a 2.1 ppb decrease.

[33] This study has sought to understand and quantify how the stratosphere influences tropospheric ozone. The scientific results can be summarized as follows:

[34] 1. Linoz v2 corrects the low bias in equatorial total column ozone found in Linoz v1, and with ECMWF IFS data our chemistry-transport model better matches the observed stratospheric column ozone.

[35] 2. Linoz is useful in diagnosing errors in stratospheric circulation for both general circulation models and assimi-

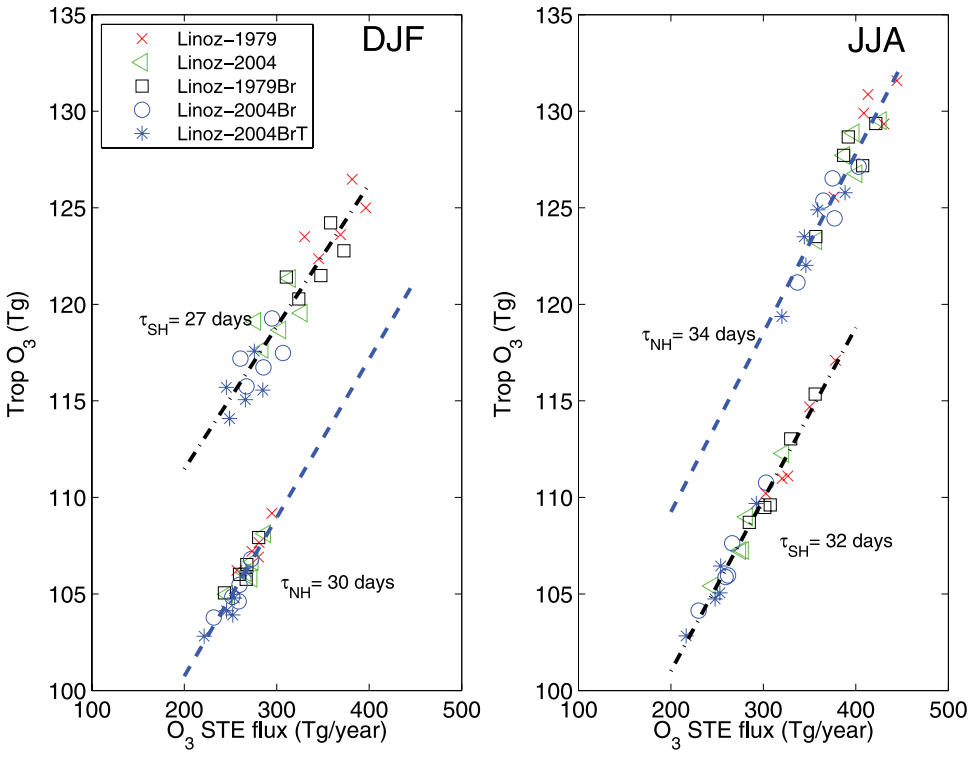

Figure 11. Mean tropospheric O_3 (Tg) versus STE O_3 flux (Tg/a) by hemisphere for DJF and JJA. The linear regression fit is shown in dashed blue line for the NH and black dash-dottted line for the SH. The slopes indicate the lifetimes of the perturbations to tropospheric ozone and are labeled in unit of days. The five different Linoz models are labeled with symbols: −1979 (red crosses), −1979Br (black squares), −2004 (green left-triangles), −2004Br (blue circles), and −2004BrT (blue asterisks).

lated winds, e.g., the change in IFS cycle to 29r2 degraded the EC L40 meteorology, but not the L60 version.

[36] 3. Observed interannual variability in total column ozone is well modeled with Linoz and the EC meteorology; however, the modeled magnitude in the SH, including QBO's influence on ozone, is twice as large. Other EC products such as ERA-40 with L60 resolution have also shown unrealistic, large SH interannual variability [*Fleming et al.*, 2007].

[37] 4. Our best estimate for the current STE ozone flux is 290 Tg/a in the NH and 225 Tg/a in the SH with interannual variability over years 2001–2005 of ±25 Tg/a and ±30 Tg/a respectively.

[38] 5. The STE shows negative anomalies over the midlatitudes during the easterly phases of the QBO and vice versa. The QBO-induced overturning circulations over midlatitudes during the easterly phase creates conditions that reduce STE.

[39] 6. The STE flux alone drives a large seasonal change in the tropospheric ozone burden with NH midlatitude peak-to-peak changes of about 7–8 DU that parallels the late summer maximum normally attributed to tropospheric photochemistry.

[40] 7. When the observed column ozone depletion from 1979 to 2004 is modeled with Linoz v2, we predict STE reductions of about 10%, corresponding to about 1 ppb in tropospheric O_3 of the Northern Hemisphere, much less than anticipated by *Fusco and Logan* [2003].

[41] **Acknowledgments.** The authors acknowledge the NASA Modelling Analysis and Prediction (MAP/GMI) program (NNG06GB84G) and the NSF Atmospheric Chemistry Program (ATM-0550234) for support of this research. The authors thank three anonymous referees for their helpful comments as well as Ivar Isaksen for providing EC/Oslo meteorological data.

References

Baldwin, M. P., et al. (2001), The quasi-biennial oscillation, *Rev. Geophys.*, *39*(2), 179–230.

Bojkov, R. D., and V. E. Fioletov (1997), Changes of the lower stratospheric ozone over Europe and Canada, *J. Geophys. Res.*, *102*(D1), 1337–1347.

Cariolle, D., A. Lasserre-Bigory, and J. F. Royer (1990), A general circulation model simulation of the springtime Antarctic ozone and its impact on mid-latitudes, *J. Geophys. Res.*, *95*(D2), 1883–1898.

Cariolle, D., and H. Teyssedre (2007), A revised linear ozone photochemistry parameterization for use in transport and general circulation models: Multi-annual simulations, *Atmos. Phys. Discuss.*, *7*, 1655–1697.

Eyring, V., D. E. Kinnison, and T. G. Shepherd (2005), Overview of planned coupled chemistry-climate simulations to support upcoming ozone and climate assessments, *SPARC Newsl.*, *25*, 11–17.

Fioletov, V. E., G. E. Bodeker, A. J. Miller, R. D. McPeters, and R. Stolarski (2002), Global and zonal total ozone variations estimated from ground-based and satellite measurements: 1964–2000, *J. Geophys. Res.*, *107*(D22), 4647, doi:10.1029/2001JD001350.

Fleming, E. L., C. H. Jackman, D. K. Weisenstein, and M. K. W. Ko (2007), The impact of interannual variability on multidecadal total ozone simulations, *J. Geophys. Res.*, *112*, D10310, doi:10.1029/2006JD007953.

Fusco, A. C., and J. A. Logan (2003), Analysis of 19701995 trends in tropospheric ozone at Northern Hemisphere midlatitudes with the GEOS-CHEM model, *J. Geophys. Res.*, *108*(D15), 4449, doi:10.1029/2002JD002742.

Hsu, J., M. J. Prather, and O. Wild (2005), Diagnosing the stratosphere-to-troposphere flux of ozone in a chemistry transport model, *J. Geophys. Res.*, *110*, D19305, doi:10.1029/2005JD006045.

Hood, L. L., and B. E. Soukharev (2005), Interannual variations of total ozone at northern midlatitudes correlated with stratospheric EP flux and potential vorticity, *J. Atmos. Sci.*, *62*, 3724–3740.

International Union of Pure and Applied Chemistry (2004), International Union of Pure and Applied Chemistry, Subcommittee on Gas Kinetic Data Evaluation, Datasheets available at http://www.iupac-kinetic.ch.cam.ac.uk/.

McPeters, R. D., G. J. Labow, and B. J. Johnson (1997), A satellite-derived ozone climatology for balloonsonde estimation of total column ozone, *J. Geophys. Res.*, *102*(D7), 8875–8886.

McPeters, R. D., G. J. Labow, and J. A. Logan (2007), Ozone climatological profiles for satellite retrieval algorithms, *J. Geophys. Res.*, *112*, D05308, doi:10.1029/2005JD006823.

McLinden, C. A., S. C. Olsen, B. J. Hannegan, O. Wild, and M. J. Prather (2000), Stratosphere ozone in 3-D models: A simple chemistry and the cross-tropopause flux, *J. Geophys. Res.*, *105*(D11), 14,653–14,665.

Michelsen, H. A., G. L. Manney, M. R. Gunson, and R. Zander (1998a), Correlations of stratospheric abundances of NO_y, O_3, N_2O, and CH_4 derived from ATMOS measurements, *J. Geophys. Res.*, *103*(D21), 28,347–28,359.

Michelsen, H. A., G. L. Manney, M. R. Gunson, C. P. Rinsland, and R. Zander (1998b), Correlations of stratospheric abundances of CH_4 and N_2O derived from ATMOS measurements, *Geophys. Res. Lett.*, *25*(15), 2777–2780.

Nassar, R., P. F. Bernath, C. D. Boone, G.L. Manney, S. D. McLeod, C. P. Rinsland, R. Skelton, and K. A. Walker (2005), Stratospheric abundances of water and methane based on ACE-FTS measurements, *Geophys. Res. Lett.*, *32*, L15S04, doi:10.1029/2005GL022383.

Nagatani, R. M., and J. E. Rosenfield (1993), Temperature, net heating and circulation, in *The Atmospheric Effects of Stratospheric Aircraft: Report of the 1992 Models and Measurements Workshop*, *NASA Ref. Publ. 1292*, edited by M. J. Prather and E. E. Remsberg, pp. A1–A47.

Prather, M. (1992), Catastrophic loss of stratospheric ozone in dense volcanic clouds, *J. Geophys. Res.*, *97*(D9), 10187–10191.

Prather, M. J., and E. E. Remsburg (Eds.) (1993), Report of the 1992 stratospheric models and measurements workshop, Satellite Beach, Fla., February 1992, *NASA Ref. Publ. 1292*, 144+268+352 pp.

Prather, M., et al. (2001), Atmospheric chemistry and greenhouse gases, in *Climate Change 2001: The Scientific Basis*, edited by J. T. Houghton et al., chap. 4, pp. 239–287, Cambridge Univ. Press, New York.

Randel, W. J., and J. B. Cobb (1994), Coherent variations of monthly mean total ozone and lower stratospheric temperature, *J. Geophys. Res.*, *99*(D3), 5433–5447.

Randel, W. J., B. A. Boville, J. C. Gille, P. L. Bailey, S. T. Massie, J. B. Kumer, J. L. Mergenthaler, and A. E. Rochem (1994), Simulation of stratospheric N_2O in the NCAR CCM2: Comparison with CLAES data and global budget analyses, *J. Atmos. Sci.*, *51*, 2834–2845.

Randel, W. J., and F. Wu (1996), Isolation of the ozone QBO in SAGE II data by singular-value decomposition, *J. Atmos. Sci.*, *53*, 2546–2559.

Randel, W. J., R. S. Stolarski, D. M. Cunnold, J. A. Logan, M. Newchurch, and J. Zawodny (1999), Trends in the vertical distribution of ozone, *Science*, *285*(5434), 689, doi:10.1126/science.285.5434.1689.

Randel, W. J., and F. Wu (2007), A stratospheric ozone profile data set for 19792005: Variability, trends, and comparisons with column ozone data, *J. Geophys. Res.*, *112*, D06313, doi:10.1029/2006JD007339.

Salawitch, R. J., D. K. Weisenstein, L. J. Kovalenko, C. E. Sioris, P. O. Wennberg, K. Chance, M. K. W. Ko, and C. A. McLinden (2005), Sensitivity of ozone to bromine in the lower stratosphere, *Geophys. Res. Lett.*, *32*, L05811, doi:10.1029/2004GL021504.

Sander, et al. (2006), Chemical kinetics and photochemical data for use in atmospheric studies, evaluation number 15, in *JPL Publication 06-2.*, Jet Propul. Lab., Pasadena, Calif.

Schoeberl, M. A., et al. (1993), The evolution of ClO and NO along air parcel trajectories, *Geophys. Res. Lett.*, *20*(22), 2511–2514.

Simmons, A., M. Hortal, G. Kelly, A. McNally, A. Untch, and S. Uppala (2005), ECMWF analyses and forecasts of stratospheric winter polar vortex breakup: September 2002 in the Southern Hemisphere and related events, *J. Atmos. Sci.*, *62*, 668–689.

Stevenson, D. S., et al. (2006), Multimodel ensemble simulations of present-day and near-future tropospheric ozone, *J. Geophys. Res.*, *111*, D08301, doi:10.1029/2005JD006338.

Stolarski, R. S., A. R. Douglass, S. Steenrod, and S. Pawson (2006), Trends in stratospheric ozone: Lessons learned from a 3D chemical transport model, *J. Atmos. Sci.*, *63*, 1028–1041.

Strahan, S. E. (1999), Climatologies of lower stratospheric NO_y and O_3 and correlations with N_2O based on in situ observations, *J. Geophys. Res.*, *104*(D23), 30,463–30,480.

Sudo, K., M. Takahashi, and H. Akimoto (2003), Future changes in stratosphere-troposphere exchange and their impacts on future tropospheric ozone simulations, *Geophys. Res. Lett.*, *30*(24), 2256, doi:10.1029/2003GL018526.

Thomason, L. W., L. R. Poole, and T. Deshler (1997), A global climatology of stratospheric aerosol surface area density deduced from Stratospheric Aerosol and Gas Experiment II measurements: 1984–1994, *J. Geophys. Res.*, *102*(D7), 8967–8976.

Thompson, D. W. J., and J. M. Wallace (1998), The Arctic Oscillation signature in the wintertime geopotential height and temperature fields, *Geophys. Res. Lett.*, *25*(9), 1297–1300.

Thornton, B. F., et al. (2005), Variability of active chlorine in the lowermost Arctic stratosphere, *J. Geophys. Res.*, *110*(D22), D22304, doi:10.1029/2004JD005580.

Thuillier, G., L. Floyd, T. N. Woods, R. Cebula, E. Hilsenrath, M. Herse, and D. Labs (2004), Solar irradiance spectra for two solar activity levels, *Adv. Space Res.*, *34*, 256–261.

Wamsley, P. R., et al. (1998), Distribution of halon-1211 in the upper troposphere and lower stratosphere and the 1994 total bromine budget, *J. Geophys. Res.*, *103*(D1), 1513–1526.

Wild, O., J. K. Sundet, M. J. Prather, I. S. A. Isaksen, H. Akimoto, E. V. Browell, and S. J. Oltmans (2003), Chemical transport model ozone simulations for spring 2001 over the western Pacific: Comparisons with TRACE-P lidar, ozonesondes, and total ozone mapping spectrometer columns, *J. Geophys. Res.*, *108*(D21), 8826, doi:10.1029/2002JD003283.

World Meteorological Organization (2007), Scientific assessment of ozone depletion, in *Global Ozone Research and Monitoring Project Report 50*, 572 pp., World Meteorol. Organ., Geneva, Switzerland.

Woodbridge, E. L., et al. (1995), Estimates of total organic and inorganic chlorine in the lower stratosphere from in situ and flask measurements during AASE II, *J. Geophys. Res.*, *100*(D2), 3057–3064.

Zeng, G., and J. A. Pyle (2005), Influence of El Nino Southern Oscillation on stratosphere/troposphere exchange and the global tropospheric ozone budget, *Geophys. Res. Lett.*, *32*, L01814, doi:10.1029/2004GL021353.

Ziemke, J. R., and S. Chandra (2003), La Nina and El Niño-induced variabilities of ozone in the tropical lower atmosphere during 1970–2001, *Geophys. Res. Lett.*, *30*(3), 1142, doi:10.1029/2002GL016387.

Ziemke, J. R., S. Chandra, B. N. Duncan, L. Froidevaux, P. K. Bhartia, P. F. Levelt, and J. W. Waters (2006), Tropospheric ozone determined from Aura OMI and MLS: Evaluation of measurements and comparison with the global modeling initiative's chemical transport model, *J. Geophys. Res.*, *111*, D19303, doi:10.1029/2006JD007089.

J. Hsu and M. J. Prather, Earth System Science, University of California, 2101 Croul Hall, Irvine, CA 92697, USA. (junoh@uci.edu)